Ferroelectrics, 447:78–85, 2013

ISSN: 0015-0193 print / 1563-5112 online
DOI: 10.1080/00150193.2013.821904

Taylor & Francis
Taylor & Francis Group

$LiNb_{1-x}Ta_xO_3$ Electronic Structure and Optical Response from *First-Principles* Calculations

A. RIEFER,* S. SANNA, AND W. G. SCHMIDT

Lehrstuhl für Theoretische Physik, Universität Paderborn, 33095 Paderborn, Germany

Ab-initio *methods are applied to investigate the electronic and optical properties of lithium niobate-tantalate mixed crystals. Thereby the GW approach based on the electronic structure obtained within density functional theory is used to obtain the electron band structure including quasi-particle effects and the linear optical response is gained form the solution of the Bethe-Salpeter equation taking excitonic and local-field effects into account. Nonlinear optical coefficients are evaluated on the level of the independent-particle approximation. It is observed that increasing the tantalum amount widens the band gap and nearly linearly affects the optical birefringence. Also some second harmonic generation coefficients vary strongly with the stoichiometry.*

Keywords LNT; $LiNbO_3$; $LiTaO_3$; birefringence; DFT; GW; BSE

I. Introduction

Due to the isomorphism between Lithium niobate (LN) and Lithium tantalate (LN) these two ferroelectrics show a number of similar properties. LN, on the one hand, is the most important electro-optic material typically used in optical modulators, acousto-optic devices, optical switches for gigahertz frequencies, laser frequency doubling, nonlinear optics, Pockels cells, optical parametric oscillators or Q-switching devices for lasers. LT, on the other hand, is often used to replace LN for applications that require shorter wavelengths.

Recently there is a strong interest in mixed LN-LT ($LiNb_{1-x}Ta_xO_3$, LNT) crystals that arises from the desire to adjust the physical properties of the ferroelectric by tuning the materials stoichiometry. While LNT belongs to the simplest ferroelectric mixed crystals, it shows peculiar physical properties. The existence of a specific composition that shows zero birefringence at room temperature is to our knowledge unique for ferroelectrics: It gives rise to an electrically polar yet optically isotropic crystal [1, 2].

While there is an obvious technological potential for LNT, and despite the wide use of LN and LT for various electro-optic and acousto-optic devices, precise information on the electronic structure and optical properties of lithium niobate-tantalate mixed crystals is scarce [3]. The difficulty to grow compositionally homogeneous crystals with traditional methods such as the Czochralski growth is certainly one of the reasons responsible for the present lack of knowledge concerning reliable materials parameters: The large separation of the solid-liquid lines in the LN-LT phase diagram complicates the crystal growth across the composition range in spite of the quite comparable radii and equal valence of Ta and Nb

Received September 28, 2012; in final form March 27, 2013.
*Corresponding author. E-mail: riefer@mail.uni-paderborn.de

and the isomorphism of the compounds. Nevertheless, homogeneous LNT crystals were recently grown [1].

The present study aims at a better understanding of the LNT materials properties by performing accurate first-principles calculations. As it was shown for other ferroelectric such as LN (see Ref. [4]), self-energy corrected density-functional theory (DFT) calculations within the GW approximation (GWA) in conjunction with the solution of the Bethe-Salpeter equation (BSE) leads to electronic band structures and optical absorption spectra with true predictive power. This computational methodology is applied in the present work to LNT. It is briefly introduced in section II. Calculated data for the electronic and optical properties (including the birefringence) of LNT are presented and discussed in section III.

II. Methodology

We follow a three-step approach to determine the electronic and optical properties computationally. (i) The ground state geometry and electronic structure of LNT crystals is obtained from density-functional theory in generalized gradient approximation (GGA). LNT crystals with compositions of x = 0, $^1/_4$, $^1/_2$, $^3/_4$, and 1 are simulated using twenty atoms within a rhombohedral $1 \times 1 \times 2$ super-cell (see Fig. 1). The equilibrium lattice constant is obtained by fitting the calculated total energy to the Murnaghan equation of state [5]. The inner degrees of freedom are determined from the consideration of the Hellman-Feynman forces, see, e.g., Ref. [6]. (ii) The electronic quasi-particle energies are determined within Hedin's GW approximation. (iii) The Bethe-Salpeter equation (BSE) is solved for coupled electron-hole excitations [7–9], thereby accounting for the screened electron-hole attraction, i.e., excitonic effects, and the unscreened electron-hole exchange, i.e., crystal local-field effects [10–12].

Calculations for the four possibilities to realize the $x = {}^1/_2$ composition within the present super-cell are performed in order to assess the error bar of our calculations with respect to local stoichiometry fluctuations and disorder. From these calculations we conclude maximum deviations of the order of 0.1 eV for transition energies and 0.01 for the birefringence.

Specifically, the Vienna ab initio simulation package (VASP) [13, 14] is used to perform the DFT-GGA calculations. Thereby the projector augmented wave (PAW) method is used to model the electron-ion interaction. The Brillouin zone integrations are replaced by a sum over a $4 \times 4 \times 4$ k-point mesh. An energy cutoff of 400 eV restricts the number of plane waves used to expand the electron wave functions. The PW91 functional [15] describes the electron-electron exchange and correlation interaction within the GGA.

In the second step, the nonlocal and energy-dependent self-energy operator Σ replaces the GGA exchange and correlation potential in order to include the electronic self-energy effects. The self-energy shifts are obtained by a perturbative solution of the quasi-particle equation. Using the implementation described in Ref. [16], Σ is calculated in the G_0W_0 approximation [17] from the convolution of the single-particle propagator G and the dynamically screened Coulomb interaction W. Thereby 1404 electronic bands are included in the calculation of the self-energy operator.

Finally, in the third step, the electron-hole interaction is taken into account. The two-particle Hamiltonian, see, e.g., Eq. (10) in Ref. [19], describes the interaction of pairs of electrons in conduction states and holes in valence states [7, 8, 17]. The diagonal part of

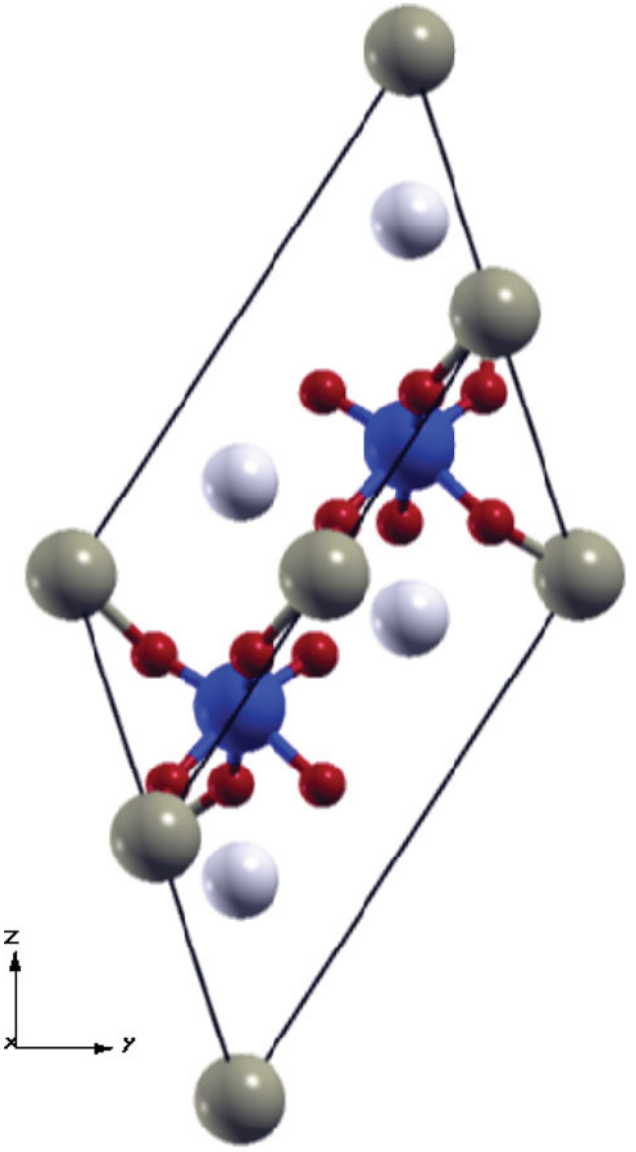

Figure 1. Rhombohedral $1\times1\times2$ super-cell used to describe $LiNb_{1-x}Ta_xO_3$ crystals with compositions x = 0, $^1/_4$, $^1/_2$, $^3/_4$, and 1. White, gray, blue, and small circles denote Li, Nb, Ta, and O atoms, respectively.

the Hamiltonian is dominated by quasi-particle transition energies, while the non-diagonal contributions arises from the screened electron-hole attraction and the unscreened electron-hole exchange. In the present work we use the model dielectric function of Bechstedt et al. [18] to describe the screening. It depends on the ε_∞ dielectric constant, which is determined here within the independent-particle approximation (IPA), see data in Fig. 2. The numerical solution of the Bethe-Salpeter equation rests on the time-evolution method proposed by one of the present authors [19, 20].

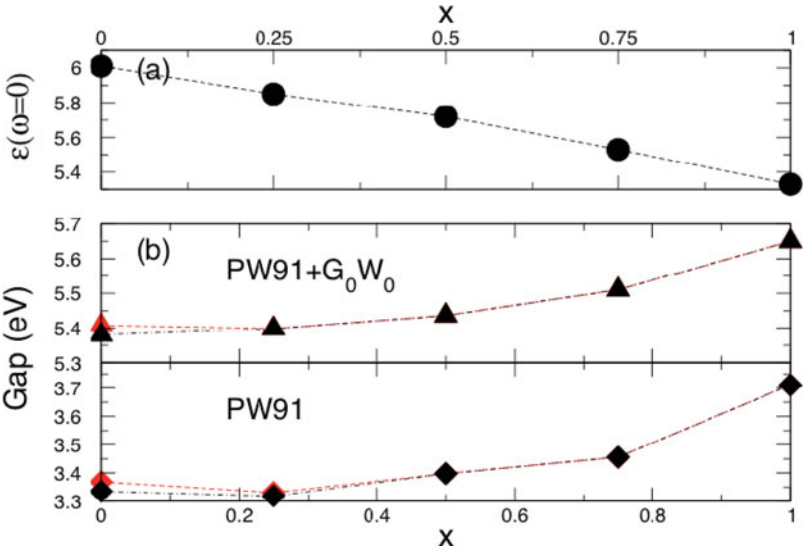

Figure 2. (a) Dielectric constant $\varepsilon_\infty = \varepsilon(\omega = 0)$ calculated within the IPA for $LiNb_{1-x}Ta_xO_3$ crystals with compositions x = 0, $^1/_4$, $^1/_2$, $^3/_4$, and 1. (b) Fundamental band gaps and band gap at the center of the Brillouin zone calculated within DFT-GGA and G_0W_0 are shown with red and black symbols, respectively.

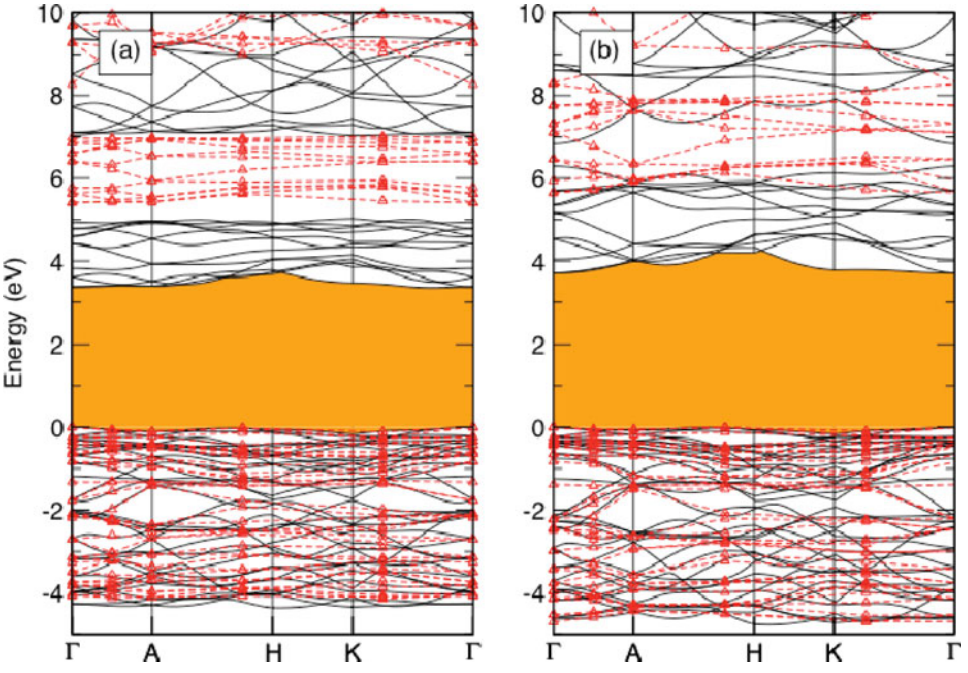

Figure 3. Electronic band structure of (a) LN and (b) LT calculated within DFT-GGA (solid lines, black) and G_0W_0 approach (red triangles). The notation of the high symmetry points follows Ref. [22]. Dashed lines guide the eye. The DFT-GGA band gap region is indicated in orange.

For the calculation of the nonlinear optical $\chi^{(2)}_{xyz}$ coefficients we follow Ref. [21]. In contrast to earlier calculations [4], however, two-band contributions are taken into account in the present work.

III. Results

The electronic structure and optical response is calculated for the ground-state geometries as determined within DFT (see also Ref. [6]). The calculated averaged dielectric constants $\varepsilon_\infty = \varepsilon(\omega = 0)$ and the PW91/G_0W_0 band gaps at the Γ-point of the Brillouin zone as well as the fundamental gaps are shown in Fig. 2. From the calculated data it is obvious that by going from LN to LT the dielectric constant is reduced nearly linear with x, starting at 6.01 and ending at 5.33. In contrast, the band gap shows some bowing. The fundamental gap obtained within G_0W_0 ranges from 5.41 eV for LN and increases to 5.65 eV for LT. The bowing parameters amount to −0.6 and −0.3 eV for the DFT-GGA and the G_0W_0 calculations, respectively. The band gap widening resulting from the inclusion of electronic self-energy effects is of the order of about 2 eV for LNT, nearly irrespective of the specific stoichiometry.

The electronic band structures calculated with DFT-GGA and G_0W_0 for LN and LT are shown in Fig. 3. Due to the structural isomorphism, the general features of the electronic

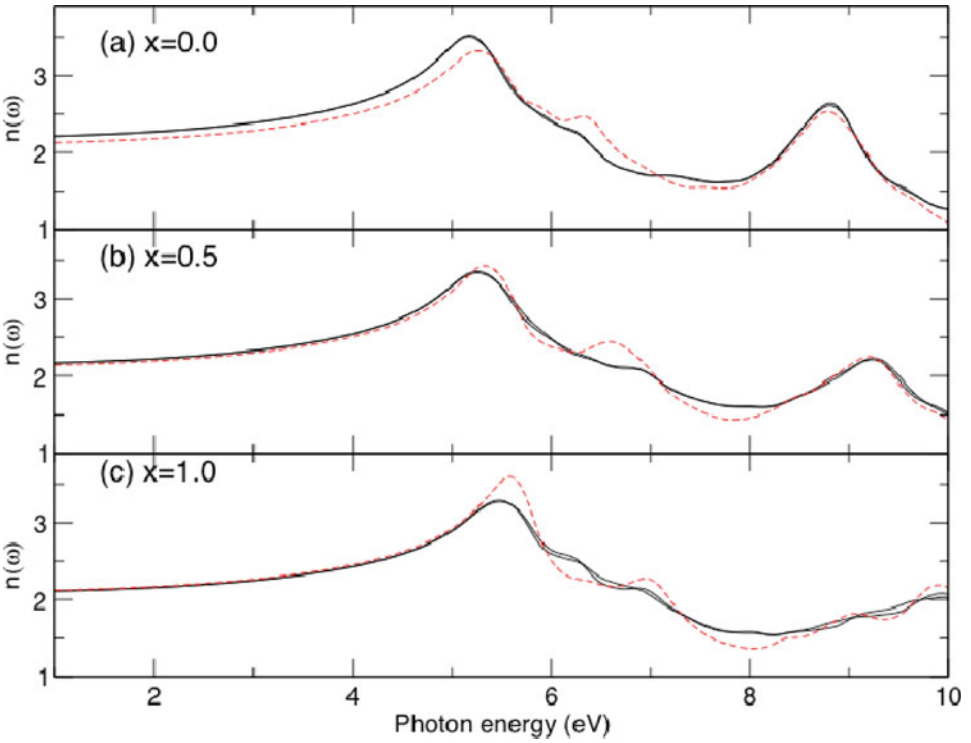

Figure 4. Refractive index obtained from solving the BSE on top of the G_0W_0 quasi-particle band structure for $LiNb_{1-x}Ta_xO_3$ with compositions x = 0, $^1/_4$, $^1/_2$, $^3/_4$, and 1 for ordinary (solid) and extraordinary (dashed) polarization (Color figure available online).

bands are similar. However, the dispersion of the LT electronic states is somewhat more pronounced than in case of LN.

The values calculated for the LN dielectric constant and transition energies are in agreement with previous work [4]. Slight deviations result from different numerical parameters and a somewhat larger lattice constant (see Ref. [6]). The reader is referred to Ref. [4] for a detailed discussion of the LN band structure. To the best of our knowledge, no experimental data or prior first-principles calculations are available for LT or mixed LNT crystals.

The refractive index $n(\omega)$ obtained from the BSE optical response calculations on top of the G_0W_0 corrected LNT band structure is shown in Fig. 4. Two features at about 5 – 8 eV and 9 – 11 eV dominate the spectra. These features blue-shift slightly with increasing tantalum amount, mainly due to the band-gap opening. The optical birefringence $\Delta n = (n_e - n_o)$, where n_e/n_o denotes the refractive index parallel/perpendicular to c, appear to be almost constant for photon energies below 5 eV and changes the sign with increasing x from negative to positive. Values for Δn are given in Fig. 5 (a) for wave length $\lambda = 632.8$ nm (1.96 eV). They depend nearly linearly on x. The data show good agreement with room temperature measurements by Wood *et al*. [2].

Finally, in Fig. 5 (b) we compare the nonlinear optical coefficients $\chi^{(2)}_{333}$, $\chi^{(2)}_{311}$, and $\chi^{(2)}_{222}$ calculated here within the IPA for a wave length of $\lambda = 1.064$ μm ($\omega = 1.17$ eV) with

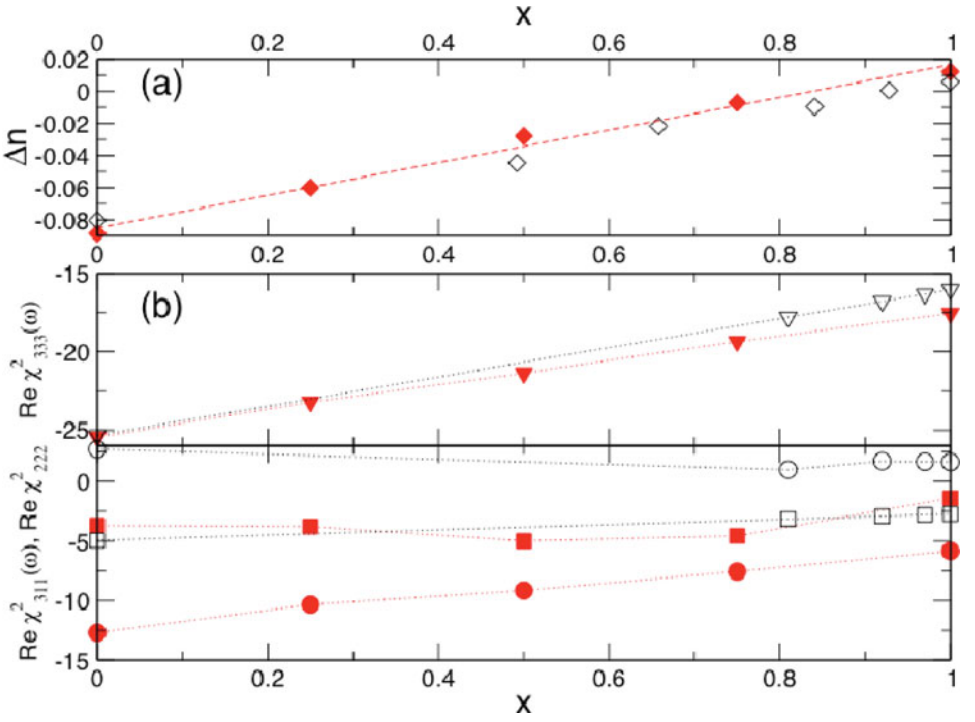

Figure 5. (a) Calculated birefringence Δn (filled diamonds) for $LiNb_{1-x}Ta_xO_3$ for $\lambda = 632.8$ nm (1.96 eV). Hollow diamonds denote experimental values obtained by Wood et al. [2]. (b) Nonlinear coefficients $\chi^{(2)}_{333}$, $\chi^{(2)}_{311}$, and $\chi^{(2)}_{222}$ (in pm/V) for $\lambda = 1.064$ μm (1.17 eV) calculated within the IPA (filled triangles, squares, and circles) compared with results from semi-empirical calculations by Xue et al. [3] (hollow symbols). Dotted lines are to guide the eyes (Color figure available online).

predictions from semi-empirical calculations by Xue *et al*. [3]. In agreement with the latter calculations, we find the magnitude of $\chi^{(2)}{}_{333}$ to decrease nearly linearly with increasing Ta content, while the stoichiometry dependence of $\chi^{(2)}{}_{311}$ is weak. In case of $\chi^{(2)}{}_{222}$ the present results deviate from the semi-empirical work [3]: The present calculations predict a stronger signal and a different sign. We carefully checked the influence of numerical parameters on the calculated SHG signal and found that in particular the inclusion of semi-core states such as Nb 4*p* electrons has an influence on the data. However, the changes observed cannot explain the deviations between the present work and the results of Ref. [3].

Acknowledgments

We gratefully acknowledge financial support from the DFG as well as supercomputer time provided by the HLRS Stuttgart and the Paderborn PC^2.

References

1. A. Bartasyte, A. Glazer, F. Wondre, D. Prabhakaran, P. Thomas, S. Huband, D. Keeble, and S. Margueron, Growth of $LiNb_{1-x}Ta_xO_3$ solid solution crystals. *Materials Chemistry and Physics*. vol. **134**, no. 2–3, pp. 728–735 (2012).
2. I. G. Wood, P. Daniels, R. H. Brown, and A. M. Glazer, Optical birefringence study of the ferroelectric phase transition in lithium niobate tantalate mixed crystals: $LiNb_{1-x}Ta_xO_3$. *Journal of Physics: Condensed Matter.* vol. **20**, no. 23, pp. 235 237–235 242 (2008).
3. D. Xue, K. Betzler, and H. Hesse, Dielectric properties of lithium niobate-tantalate crystals. *Solid State Communications*. vol. **115**, no. 11, pp. 581–585 (2000).
4. A. Riefer, S. Sanna, A. V. Gavrilenko, and W. G. Schmidt, "$LiNbO_3$ linear and nonlinear optical response from first-principles calculations." Applications of Ferroelectrics (ISAF/PFM), 2011 International Symposium on Piezoresponse Force Microscopy and Nanoscale Phenomena in Polar Materials (2011).
5. F. D. Murnaghan, The Compressibility of Media under Extreme Pressures. *Proceedings of the National Academy of Sciences of the United States of America*. vol. **30**, no. 9, pp. 244–247 (1944).
6. S. Sanna, A. Riefer, S. Neufeld, G. Berth, A. Widhalm, A. Zrenner, and W. G. Schmidt, "Vibrational fingerprints of $LiNbO_3$-$LiTaO_3$ mixed crystals." International Symposium on Applications of Ferroelectrics (ISAF), European Conference on the Applications of Polar Dielectrics (ECAPD) and International Symposium on Piezoresponse Force Microscopy and Nanoscale Phenomena in Polar Materials (PFM). (2012).
7. S. Albrecht, L. Reining, R. Del Sole, and G. Onida, "*Ab Initio* calculation of excitonic effects in the optical spectra of semiconductors." *Phys. Rev. Lett*. vol. **80**, pp. 4510–4513 (May 1998).
8. L. X. Benedict, E. L. Shirley, and R. B. Bohn, "Optical absorption of insulators and the electron-hole interaction: An *Ab Initio* calculation." *Phys. Rev. Lett*. vol. **80**, pp. 4514–4517 (May 1998).
9. M. Rohlfing and S. G. Louie, "Excitons and optical spectrum of the Si(111) $-$ (2 $\times$ 1) surface." *Phys. Rev. Lett*. vol. **83**, pp. 856–859 (Jul 1999).
10. L. J. Sham and T. M. Rice, "Many-particle derivation of the effective-mass equation for the wannier exciton." *Phys. Rev.* vol. **144**, pp. 708–714 (Apr 1966).
11. W. Hanke and L. J. Sham, "Local-field and excitonic effects in the optical spectrum of a covalent crystal". *Phys. Rev. B*. vol. **12**, pp. 4501–4511 (Nov 1975).
12. W. Hanke, and L. J. Sham, "Many-particle effects in the optical spectrum of a semiconductor." *Phys. Rev. B*. vol. **21**, pp. 4656–4673 (May 1980).
13. P. E. Blöchl, "Projector augmented-wave method." *Phys. Rev. B*. vol. **50**, pp. 17953–17 979 (Dec 1994).
14. G. Kresse, and J. Furthmüller, "Efficient iterative schemes for ab initio total-energy calculations using a plane-wave basis set." *Phys. Rev. B*. vol. **54**, no. 16, pp. 11169–11186 (Oct. 1996).

15. J. P. Perdew, J. A. Chevary, S. H. Vosko, K. A. Jackson, M. R. Pederson, D. J. Singh, and C. Fiolhais, "Atoms, molecules, solids, and surfaces: Applications of the generalized gradient approximation for exchange and correlation." *Phys. Rev. B*, vol. **46**, pp. 6671–6687 (Sep 1992).
16. M. Shishkin, and G. Kresse, "Implementation and performance of the frequency-dependent GW method within the PAW framework." *Phys. Rev. B*, vol. **74**, p. 035101 (Jul 2006).
17. M. S. Hybertsen, and S. G. Louie, "Electron correlation in semiconductors and insulators: Band gaps and quasiparticle energies." *Phys. Rev. B*, vol. **34**, no. 8, pp. 5390–5413 (Oct. 1986).
18. F. Bechstedt, *Festköperprobleme / Advances in Solid State Physics*. Vieweg: Braunschweig/Wies baden, 1992, vol. **32**, p. 161.
19. W. G. Schmidt, S. Glutsch, P. H. Hahn, and F. Bechstedt, "Efficient $O(N^2)$ method to solve the Bethe-Salpeter equation." *Phys. Rev. B*. vol. **67**, p. 085307 (Feb 2003).
20. P. H. Hahn, W. G. Schmidt, and F. Bechstedt, "Bulk excitonic effects in surface optical spectra." *Phys. Rev. Lett*. vol. **88**, p. 016402 (Dec 2001).
21. R. Leitsmann, W. G. Schmidt, P. H. Hahn, and F. Bechstedt, "Second-harmonic polarizability including electron-hole attraction from band-structure theory." *Phys. Rev. B*. vol. **71**, p. 195209 (2005).
22. W. G. Schmidt, M. Albrecht, S. Wippermann, S. Blankenburg, E. Rauls, F. Fuchs, C. Rödl, J. Furthmüller, and A. Hermann, "$LiNbO_3$ ground- and excited-state properties from first-principles calculations." *Phys. Rev. B*. vol. **77**, pp. 035106:1–035106:6 (Jan 2008).